RSC Advances

PAPER

View Article Online
View Journal | View Issue

Cite this: *RSC Adv.*, 2022, **12**, 21004

Structural evolution of soil aggregates in a karst rocky desertification area

Chunjie Li[ac] and Shili Guo *[b]

Desertification and karst landforms are widespread in the water source area of the middle route project of south-to-north water diversion in China. Soil erosion processes directly influence water quality in the water source area and contribute sediments to the bottom of the water reservoir. This study investigates soil evolution over time by sampling a slope surface and discusses associated changes in soil structure, physical and chemical properties, and mineral associations. Changes in soil aggregate structures with slope surface direction and mineral association evolution are observed. The compositions of the main soil minerals and elements are determined using scanning electron microscopy, and X-ray energy spectrum and X-ray diffraction analyses. The results reveal that (1) the evolution of soil aggregates is consistent with evolutionary trends in soil elements and mineral associations. (2) The ultra-microstructure of soil aggregate indicates the soil development stage and condition, while mineral associations indicate the soil development stage along the soil chronosequence. This study increases the understanding of land surface processes in the study area and the soil development, forming and biogeochemical processes in karst rocky desertification areas.

Received 8th May 2022
Accepted 13th July 2022

DOI: 10.1039/d2ra02901d

rsc.li/rsc-advances

1. Introduction

Across the world, soil degradation and erosion are potential threats to food safety.[1] Sedimentation by erosion products is one of the main problems in water reservoir management.[2] Topography has a great influence on soil properties and distributions due to the effects of the gradient, hydrodynamics, erosion and sedimentation.[3–5] The importance of time sequences in research into soil forming has been recognized in previous studies.[6–9] Soil development refers to changes in soil form, composition and mineralogical properties over time.[10,11] Different positions in a slope surface can indicate the soil evolutionary process over time. As soil erosion and chemical weathering processes develop, soil aggregate structures and mineral compositions may change. The evolution of soil aggregate elements and mineralogical compositions results from a complicated feedback effect of geochemistry and land-form processes in internal soil layers and boundaries.[12,13]

This study investigates the water source area at the mid-line of China's south-to-north water transfer project, which is located in a transitional zone between the subtropical and warm temperature zones of the East Asian hinterland. The area features wide rocky desertification and karst landforms. Rocky desertification can aggravate regional soil erosion and water and soil losses.[14] Soil degradation may be accompanied by changes in the structures and functions of soil aggregates, and some substances will be taken to water source areas by hydrological process, resulting in reservoir sedimentation, deterioration in water quality, damage to hydrophytic habitats and other environmental problems.[15–17] The structure and properties of soil aggregates deeply influence soil fertility and erosion processes.[18] The presence of aggregates is a key soil property for increasing soil infiltration and decreasing soil erosion and runoff.[19] Soil aggregates, which are cemented by inorganic and organic matter, control crop growth and development, water permeation, aeration and drainage, and create habitats for edaphone soil communities.[20] In recent years, some scholars have studied the physical and chemical properties of soil in karst regions. However, there has been little research on the evolution of the ultrastructure of soil aggregations and mineral associations over time along slope surfaces. In this study, we aim to demonstrate that the ultrastructure and mineral associations of aggregates undergo significant changes and evolve over time as soil development, soil-forming processes, soil erosion and chemical weathering proceed.[21] It is necessary to conduct longitudinal research in order to verify the influences of soil erosion and chemical weathering on the ultrastructure and mineral compositions of soil aggregations over time. This research used scanning electron microscopy (SEM) to represent aggregate ultrastructure, energy-dispersive X-ray spectroscopy (EDS) to analyse changes in soil elements, and X-ray diffraction

[a]*School of Geography and Tourism, Nanyang Normal University, Wolong Road No. 1638, Nanyang 473061, China*

[b]*School of Economics, Southwestern University of Finance and Economics, 555, Liutai Avenue, Wenjiang District, Chengdu, Sichuan, 611130, China. E-mail: guoshili@swufe.edu.cn; Tel: +86-13688134484*

[c]*Henan Key Laboratory of Ecological Security for Water Source Region of Mid-line of South-to-North Diversion Project, Wolong Road No. 1638, Nanyang 473061, China*

(XRD) to analyse changes in mineral associations. It expands the understanding of biogeochemical cycles and stages in rocky desertification and karst regions at the microscale, thus providing scientific reference and theoretical support for protecting the ecological environments of water source areas. Additionally, this research provides a reference on soil-forming processes, soil erosion and sedimentation, and biogeochemical cycles in rocky desertification and karst regions, and for researching land surface processes in China's climatic transitional zone of the Qinling Mountains-Huaihe River.

2. Materials and methods

2.1 Overview of research area

The research area is located in the transitional zone between the subtropical and warm temperate zones. It is a geographically-typical south–north transitional zone of East Asian climate and features wide, rocky, desertification landforms. It has a limestone marine stratum and the area of rocky desertification is 1526 km^2. Located in central China (32° 36′–33° 48′ N, 110° 59′–111° 49′ E; Fig. 1), Danjiangkou Reservoir is a water source area at the Middle Route Project of South-to-North Water Diversion in China, which is one of the largest artificial water transfer projects in the world. This region features a subtropical monsoon climate and prevailing westerly winds. The annual average temperature is 15.7 °C. The average precipitation from May to September is 749.3 mm, which is 80% of the annual total. The soil erosion in the Danjiangkou Reservoir of study area is relatively serious. According to the results of the second remote sensing survey of soil erosion in China, the average soil erosion modulus is about 3517 t km^{-2} a^{-1}.[21] The land use types in the study area are: sloping farmland, forest land, wasteland, paddy fields, *etc.* The local government has issued a bill prohibiting grazing and land reclamation in areas with large slopes.

2.2 Acquisition and processing of soil samples

We designed sampling points at positions A, B, C, D, E and F (Fig. 2). The coordinates of point A were 32° 51′ 30.8″ N, 111° 34′ 36.9″ E, which is 381.3 m above sea level. Due to soil erosion and

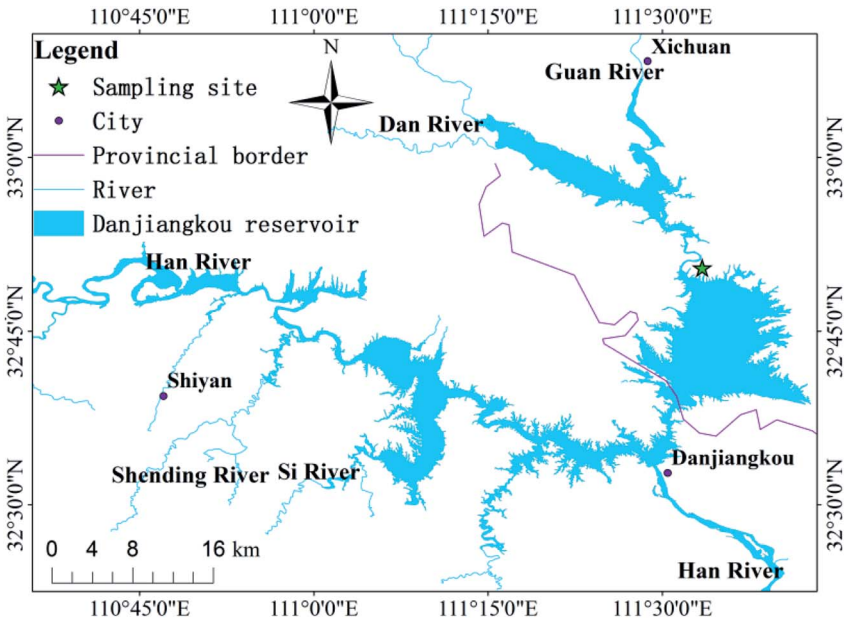

Fig. 1 Map of China showing the location of the study area; and the sampling sites in the Danjiangkou Reservoir.

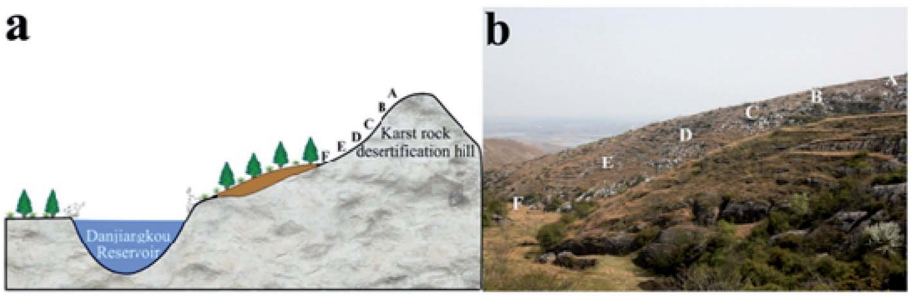

Fig. 2 Landscape map and soil chronosequence of sampling points, positions A, B, C, D, E and F decreasing altitude along the slope.

transported deposits, point A exhibits an early stage of the soil-forming process while point F exhibits a late stage. Points A, B, C, D, E and F were selected to represent the complete time sequence of the soil-forming process. We collected soil samples at 0–5 cm depth from slope surfaces with altitude down the slope. We removed dry branches and fallen leaves before collecting topsoil samples, put them in aluminium boxes, and took them to a laboratory. Samples were frozen at −80 °C for 1 h, then placed in a freeze-dryer, where they were vacuumized and dried at low temperature (0.05 MPa at −50 °C for 24 h). We dried collected soil samples at room temperature, removed plant roots, dry branches and fallen leaves, filtered coarse particles from the soil with a 2 mm mesh screen, and used SEM and X-ray spectroscopy to analyse them. In the preliminary treatment

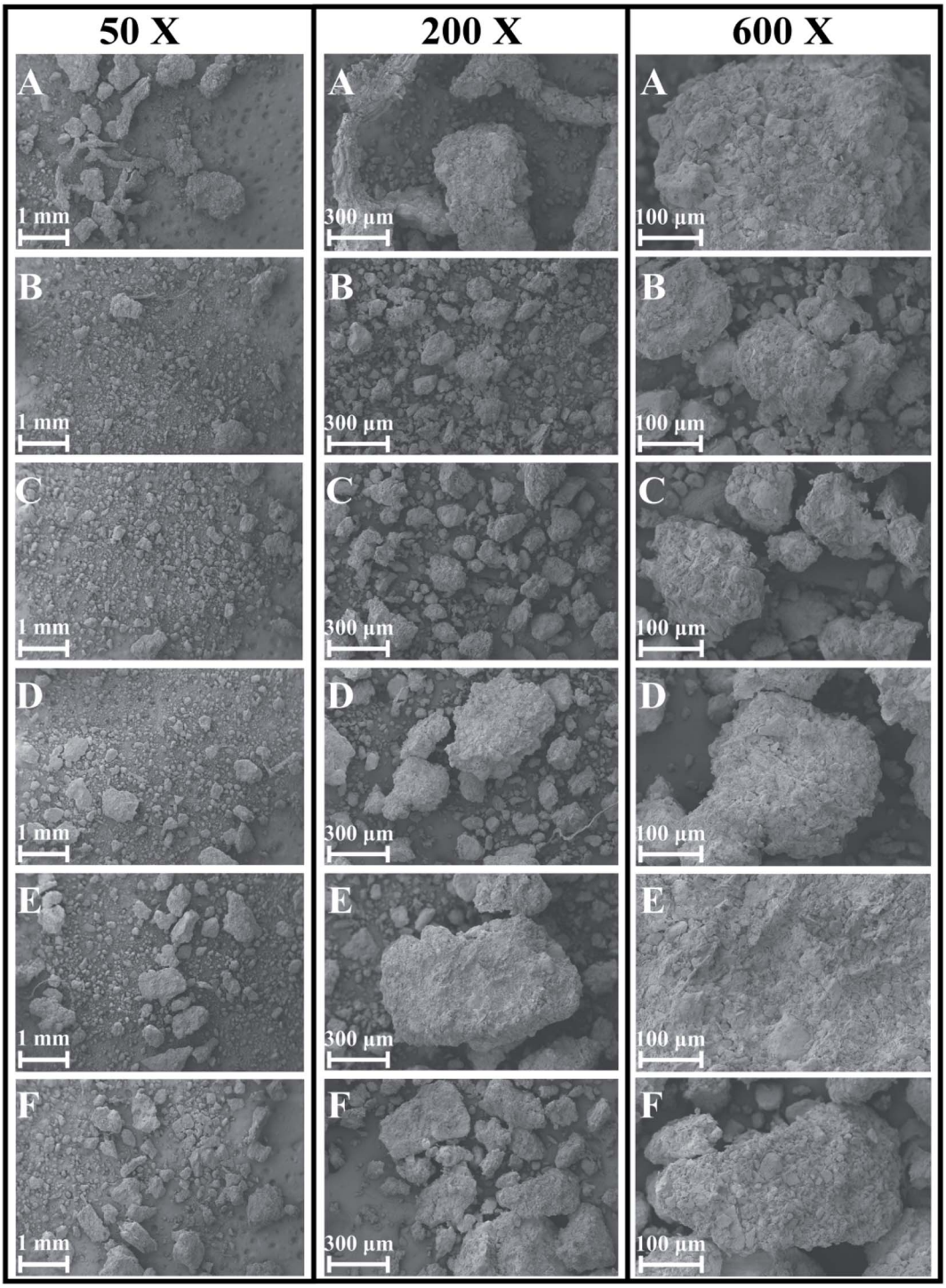

Fig. 3 SEM photographs of soil particles at 50×, 200× and 600× magnification along the soil chronosequence, (A–F) represent the locations of sampling points in Fig. 2.

process, we used H_2O_2 (30%, analytically pure) to remove organic matter from the soil and obtain scattered soil particles. The particles were then dried and ground finely in an agate mortar. They were then filtered through a 400 mesh screen and X-ray diffraction technique was used to analyse their mineral compositions.

2.3 SEM-EDS analysis for soil samples

SEM has been used to study the microstructures of soil aggregates. The operating principle of SEM is that a narrow electron beam rasters over the object's surface and secondary electrons are generated from each point of sample surface. The detector captures the secondary electrons to generate an electronic

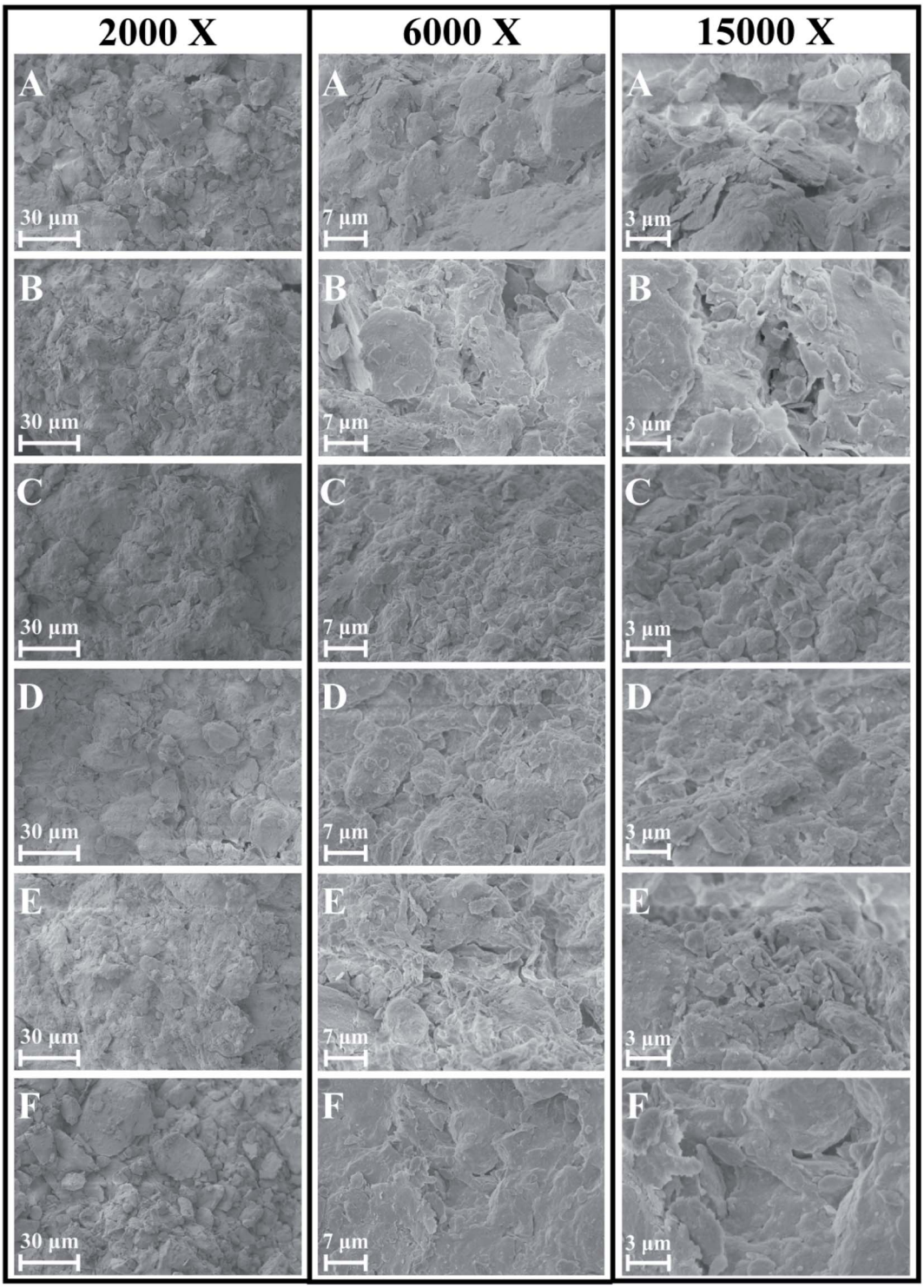

Fig. 4 SEM photographs of soil aggregates at 2000×, 6000× and 15 000× magnification along the soil chronosequence, (A–F) represent the locations of sampling points in Fig. 2.

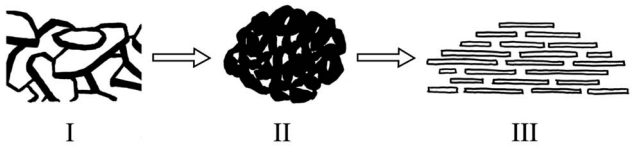

Fig. 5 Evolution of soil aggregates ultrastructure along the soil chronosequence.

signal that provides a visual image. Soil powder was mounted in a conductive adhesive and sprayed with gold powder by an ion sputtering instrument for testing in the SEM (Zeiss Evo18).

An EDS instrument (Bruker Nano Berlin, Germany, XFlash 6|30) with an acceleration voltage of 10 kV was used. The main elements represented by this detector include O, Si, Al, Fe, Ca, Na, K, Mg and P. For the XRD analyses, the operating conditions were an electron beam acceleration voltage of 10 kV, beam current of 0.2 nA, working distance of 80 mm and X-ray angle of emergence of 35°. The signal was recorded in channel 4096 for a counting time of 40 seconds and detection thickness of 0.45 mm. To calibrate the EDS results, we used standardless quantification method. This method relied on peak-to-background ZAF evaluation (P/B-ZAF) and provided reliable quantification results.

2.4 Mineral analysis for soil samples

X-ray diffraction technique was used to analyse soil minerals. We processed samples into powder chips and analysed them

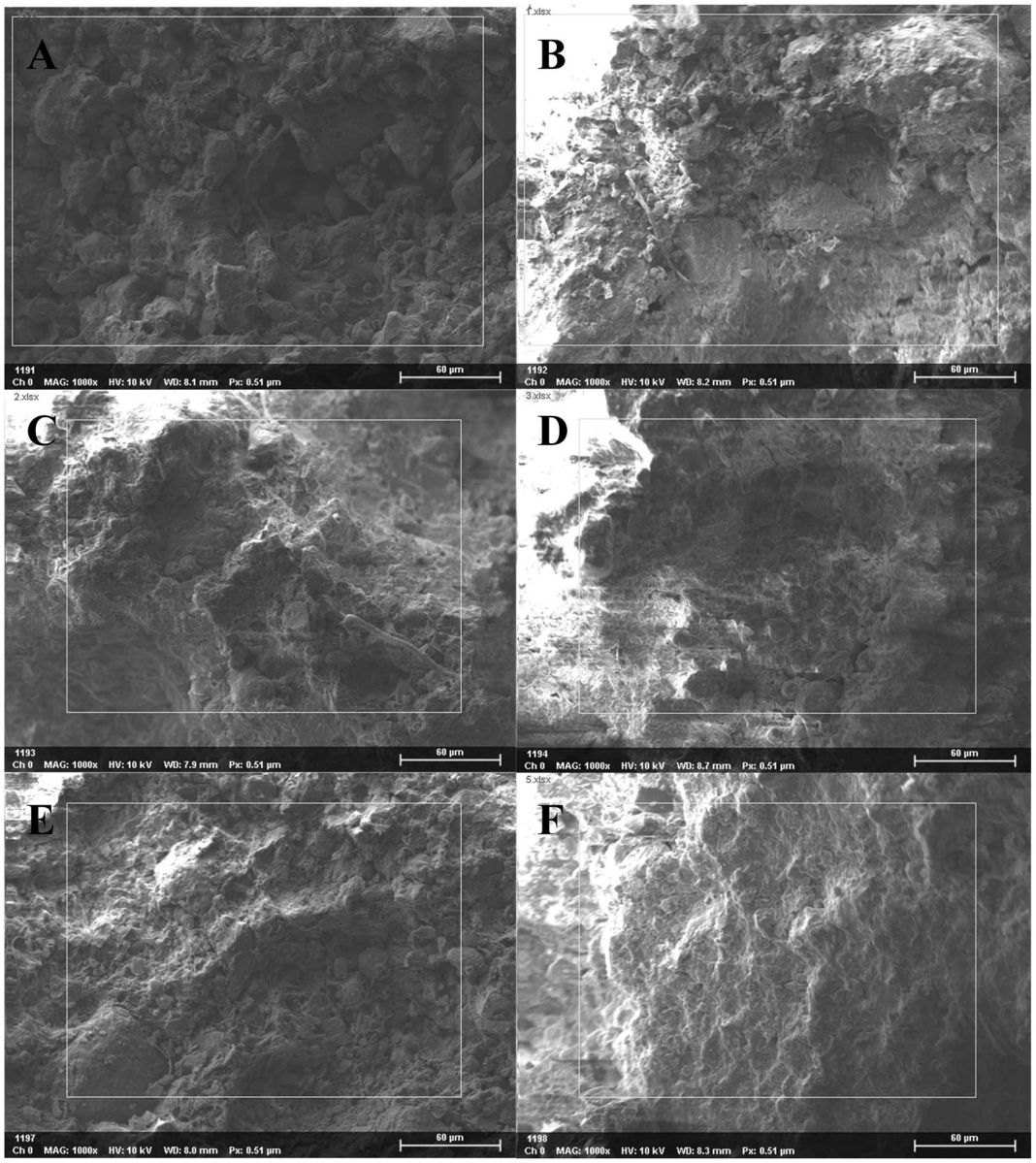

Fig. 6 SEM-EDS results with the area under exposure to electron beam along the soil chronosequence, (A–F) represent the locations of sampling points in Fig. 2.

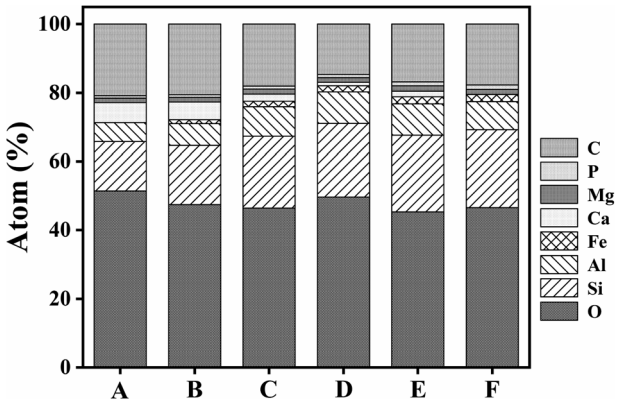

Fig. 7 Variation of atomic fraction of soil element by EDS along the soil chronosequence.

with an X-ray diffractometer (Rigaku Smartlab 9 kW Full Auto X-ray Diffractometer). The measurement conditions included a Cu Kα target, filtering of graphite monochromator; tube voltage of 40 kV; current of 150 mA; scanning range of 5°–80° (2θ; scanning speed of 6° min^{-1}). The diffraction peaks obtained from X-ray diffraction (XRD) were processed using Jade software and compared with standard PDF cards to obtain phase analysis results. Based on the thermal isolation method, we measured the integral intensity of certain diffraction peaks of clay and various non-clay minerals in the diffractogram to directly calculate their total quantities. The calculation formula is:

$$X_i = \left[\frac{I_i}{K_i} \Big/ \left(\sum \frac{I_i}{K_i}\right)\right] \times 100\%$$

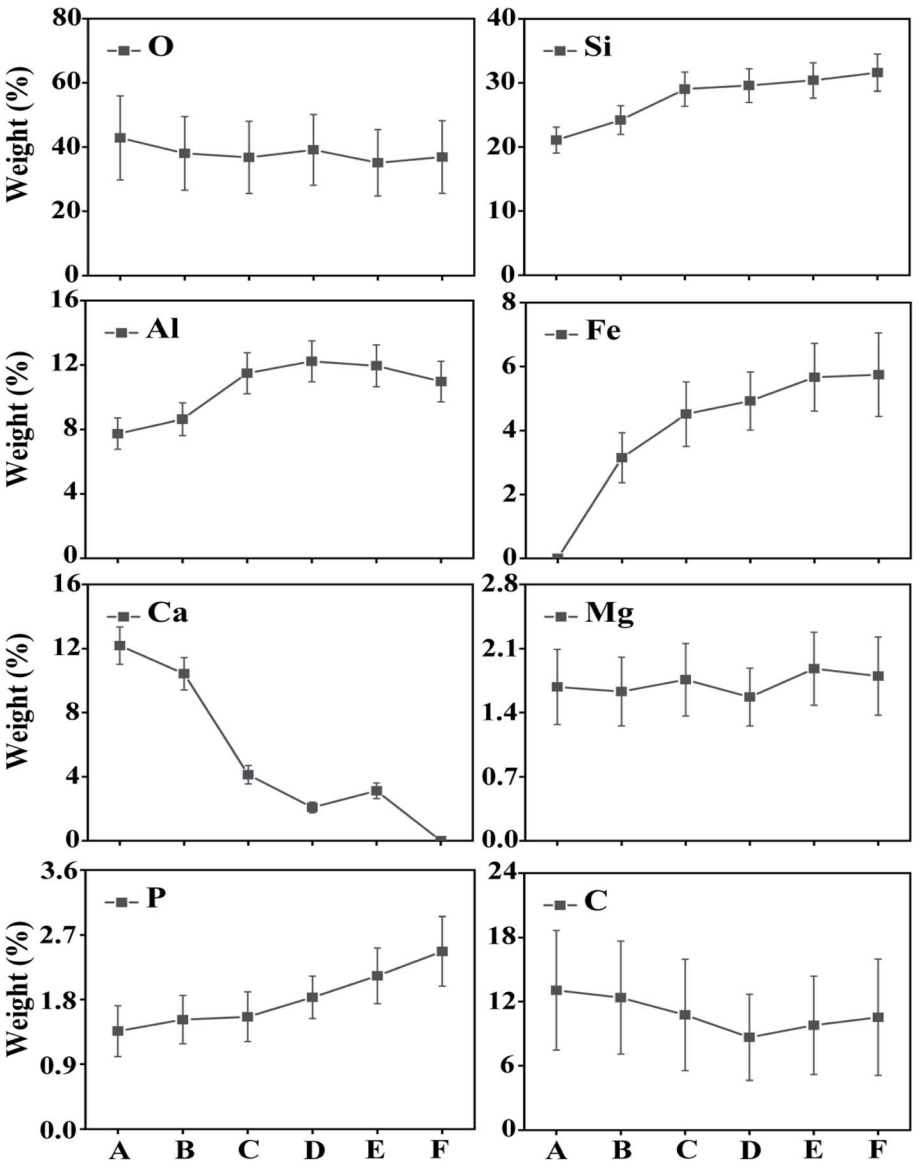

Fig. 8 Variation of soil mass abundance by EDS along the soil chronosequence.

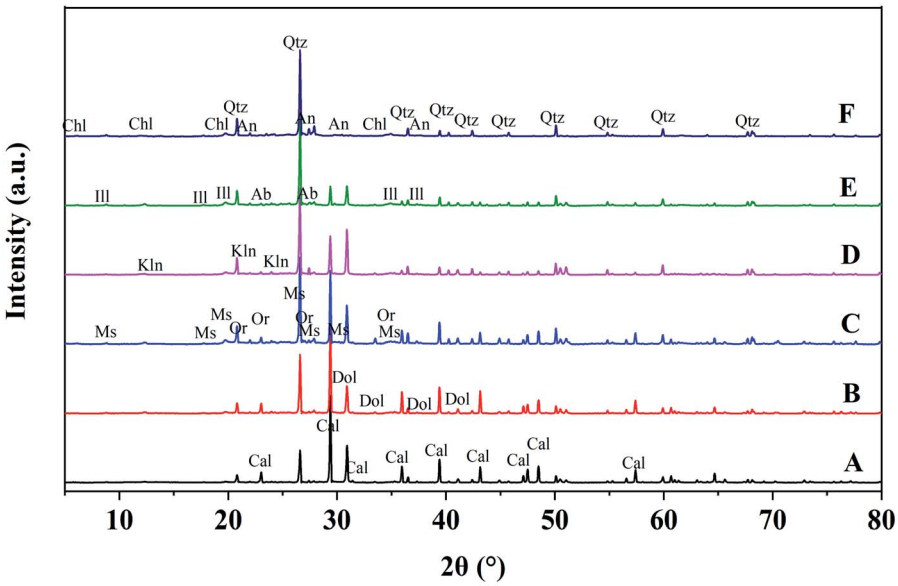

Fig. 9 X-ray diffractogram patterns (Cu Kα radiation) and mineral change of soil aggregates along the soil chronosequence (Cal = calcite; Chl = chlorite; Dol = dolomite; Ill = illite; Kln = kaolinite; Ms = muscovite; Or = orthoclase; Qtz = quartz; An = anorthite; Ab = albite).

Table 1 Mass fraction of soil mineral using XRD with standard deviation (%)

Mineral	A	B	C	D	E	F
Calcite	52.7 ± 2.1	46.1 ± 1.9	27.4 ± 0.8	17.4 ± 1.5	10.5 ± 0.4	0.4 ± 0.3
Chlorite	2.3 ± 0.8	2.6 ± 0.5	4.1 ± 0.5	3.2 ± 0.6	5.3 ± 0.4	6.2 ± 0.3
Dolomite	17.5 ± 2.6	14.5 ± 1.4	16.8 ± 1.1	23.0 ± 1.5	12.3 ± 0.6	2.8 ± 0.3
Illite	4.0 ± 0.6	9.0 ± 0.6	17.1 ± 0.6	14.3 ± 0.6	21.8 ± 0.4	26.0 ± 0.5
Kaolinite	2.9 ± 0.9	4.7 ± 0.7	7.5 ± 0.7	5.4 ± 0.8	8.2 ± 0.4	5.2 ± 0.5
Muscovite	0.6 ± 0.5	0.8 ± 0.7	1.4 ± 0.8	2.1 ± 1.0	2.1 ± 0.5	2.9 ± 0.6
Orthoclase	0.7 ± 0.6	0.6 ± 0.6	1.7 ± 0.9	1.8 ± 0.9	1.9 ± 0.6	1.6 ± 0.7
Quartz	14.2 ± 1.0	14.9 ± 0.4	14.9 ± 0.3	22.8 ± 0.4	26.2 ± 0.3	29.8 ± 0.2
Anorthite	3.1 ± 1.0	4.0 ± 0.9	4.2 ± 0.8	5.6 ± 0.8	8.6 ± 0.4	16.8 ± 0.7
Albite	1.8 ± 1.1	2.7 ± 0.6	4.9 ± 0.6	4.4 ± 0.7	3.1 ± 0.5	8.4 ± 0.6

where X_i refers to the composition of mineral i in the sample (%); K_i refers to the reference intensity of mineral i; and I_i is the intensity of the diffraction peak for mineral i.

2.5 Data analysis and mapping

Data were analysed in SPSS 15.0 software. A map was generated using ArcGIS 10.0 (ESRI, Redlands, CA, USA: https://www.esri.com/software/arcgis).

3. Results

3.1 Changes in soil aggregation structure

The soil had different grain diameters and showed single-particle and aggregate structures under SEM. According to the SEM analysis, the soil structure changed significantly in the direction of the slope surface. Under low magnification, we found that the soil particle size generally tended to decline and then increase from point A to point F (Fig. 3).

Under high magnification, we observed a non-directional microstructures at points A and B (top of slope), flocculent microstructures at points C and D (middle of slope) and directional and layered microstructures at points E and F (bottom of slope; Fig. 4 and 5). Therefore, the microstructure of the soil changed dramatically over time.

3.2 Changes in the main elements

This study analysed changes in the geochemical elements of soil aggregates using X-ray energy spectra. According to the results, as a whole, the proportions of elements O, Si and Al were high, that of Ca tended to decline along the slope surface, while that of Fe tended to increase. The presence of high Al and Si contents was extremely obvious, because Si compounds are relatively stable in nature. Contents of C tended to decline and then increase with altitude down the slope, while Mg and O had slight changes. Element P tended to increase and indicate an enrichment status of soil nutrient (Fig. 6–8). Therefore, the

chemical elements in the soil showed extremely clear migration over time.

3.3 Evolution in soil mineral associations

According to X-ray diffraction analysis, the soil minerals included calcite, chlorite, dolomite, illite, kaolinite, muscovite, orthoclase, quartz, anorthite and albite. At points A and B (top of slope), the main minerals included calcite, quartz and dolomite; at points C and D (middle of slope), there was calcite, quartz, dolomite and illite; while at points E and F (bottom of slope), there was illite, quartz and anorthite. Meanwhile, the proportions of chlorite, albite and muscovite tended to increase with altitude down the slope. The content of calcite in soil at the bottom of the slope was less than 1% (Fig. 9, Table 1).

4. Discussion

4.1 Evolution of soil aggregate structure in soil-forming process

In this research, we attempted to demonstrate that the microstructures, elements and mineral associations of aggregates undergo significant changes as they evolve over time during soil development, soil-forming processes, soil erosion and chemical weathering. Due to soil erosion, the soil-forming process is in an early stage at the top of the slope (point A) and in a late stage at the bottom of the slope (point F). Positions A, B, C, D, E and F on the slope surface represent different soil-forming times. According to SEM analysis, the microstructure of soil changed significantly with decreasing altitude along the slope. Under low magnification, we found that soil particle sizes generally tended to decline and then increase. Therefore, changes during the soil-forming process in the research area can be represented by changes in particle size. Under high magnification, we observed a non-directional ultrastructure at points A and B (top of slope) in the first stage; flocculent ultrastructure at points C and D (middle of slope) in the second stage and directional and layered ultrastructure at points E and F (bottom of slope) in the third stage (Fig. 4 and 5). Therefore, cementation and recrystallization may occur from the middle of the slope to the bottom of the slope. The content of Al first increases and then decreases, which shows that an Al enrichment effect exists at the bottom of the slope. The flocculent structures of soil particles may be related to Al; small substances produced by chemical erosion can react with Al to generate flocculent precipitates, then cementation occurs to produce such structures.

Soil colloids are generally considered as particles with effective diameters of 10 nm to 10 μm. The smallest colloids are larger than dissolved macromolecules. Soil colloids are the most active part of soil and determine its chemical and physical properties to a large extent.[22–24] Soil containing colloidal substances feature agglomeration,[20] which results from the realignment, flocculation and cementation of particles.[25] Aggregates may initially form through the gradual combination of clay, soil organic matter (SOM) and positive ions, or be a transitional product of macro-aggregates.[26] The complicated interaction among aggregates can be coordinated or damaged.[27] Calcium carbonate and clay particle are important inorganic cementing agents in soil. Element Fe can also cement and flocculate clay particles to a certain extent. Clay particles gather through realignment and flocculation. The positive ions, for example, Si^{4+}, Fe^{3+}, Al^{3+} and Ca^{2+}, stimulate the precipitation of compounds that are used as bonding agents for primary particles.[27] Organic colloids are more chemically active and generally have a greater influence on soil properties per unit weight than inorganic colloids. In soil with a low organic content, coordinated compounds are formed through the connection of polyvalent metal cations, so the ultrastructure of soil aggregates is not stable. Soil aggregates are cemented by organic and inorganic matter and are the basic structural units of soil. Furthermore, soil aggregates are involved in soil structural, physical, chemical and biological processes.[28]

4.2 Evolution of aggregate elements and mineral associations during the soil-forming process

Biochemical weathering is the main form of interaction between mainland surface spheres and is a key step in the biogeochemical circulation of elements. As a whole, the proportions of O, Si and Al were high (Fig. 6–8), which is consistent with the basic geochemical rules of elements. Through ion exchange, small particles are transported by water flow, while coarse particles stay in their original positions and fine particles fill in voids in incompact weathering crust to form cemented substances. Contents of Ca tended to decline along the slope surface,

Table 2 Linear correlation matrix for atomic abundance of soil

	O	Si	Al	Fe	Ca	Mg	P	C
O	1.000							
Si	−0.715	1.000						
Al	−0.572	0.935[a]	1.000					
Fe	−0.781[b]	0.980[a]	0.903[a]	1.000				
Ca	0.532	−0.962[a]	−0.889[a]	−0.901[a]	1.000			
Mg	−0.839[b]	0.657	0.534	0.634	−0.543	1.000		
P	−0.614	0.844[b]	0.646	0.824[b]	−0.850[b]	0.676	1.000	
C	0.237	−0.807[b]	−0.919[a]	−0.758[b]	0.834[b]	−0.241	−0.572	1.000

[a] Correlation is significant at the 0.01 level (2-tailed). [b] Correlation is significant at the 0.05 level (2-tailed).

consistent with the processes of migration and loss. Contents of Fe tended to increase, while the proportions of Fe, P and Mg were relatively small (Fig. 6 and 7). A phenomenon of enriched Si, Al and Fe was obvious. According to Table 2, the correlations between Si, Al and Fe were high. The changes in proportions of Fe and Al were related to the ultrastructure of the soil.[29] Contents of Si tended to increase, because Si compounds are relatively stable in nature (Table 2). As the soil-forming process and soil weathering and vegetation development proceed, the acidity of soil increases and minerals such as calcite and dolomite are dissolved. In the preliminary and middle periods of soil weathering and development, the weathering of carbonate minerals is generally the main development process.[30] Furthermore, the decline in Ca content is also related to dissolution and migration of calcite under the action of weakly-acidic rainwater.[31] More Ca will be adsorbed on the surfaces of soil colloids due to dissolved calcium carbonate, which will increase scattered soil colloids and form a more incompact soil colloid apparent structure.[32] The correlation analysis showed that: (1) Si and Al were positively correlated. (2) Si and Fe were positively correlated. (3) Al and Fe were positively correlated. (4) Si and Ca were negatively correlated. (5) Al and Ca were negatively correlated. (6) Al and C were also negatively correlated (Table 2). Element P is key to life on earth.[33] The constitutional changes in P in soil are closely related to soil development, vegetation development and the migration of pollutants. As soil develops, the adsorption capacity of clay surfaces for P also increase constantly.[34] Element P tended to increase over time in the research area, indicating an enrichment state. This result provides evidence for a P migration process in the water source area and provides a reference for governing non-point-source P pollution. P combined with Ca and Al declines as organic phosphorus increases during the soil development process.[35] Generally, the phenomenon of enriched Al, Si and Fe was obvious, while overall changes in Mg and O were not significant. Element C tended to decline firstly and then increase, and a position in the middle of the slope will not promote the accumulation of organic carbon. Element C will exist in the form of organic carbon, but also in the form of inorganic carbon. The inorganic carbon exists in soil in the form of original minerals and secondary minerals. Soil aggregates are sites for the storage of soil carbon and are extremely important for soil carbon fixation and fertility. Humus is a cemented substance that can form stable aggregates. Organic carbon indirectly influences the soil structure *via* carbonates, and increases in organic carbon will result in the decomposition of carbonates in soil.[27]

The soil-forming process results in changes in soil properties and is accompanied by the continuous weathering of soil minerals. Clay minerals are crystalline (although some are formless) and generally have special physical and chemical ultrastructure. Soil minerals include calcite, chlorite, dolomite, illite, kaolinite, muscovite, orthoclase, quartz, anorthite and albite. The main mineral compositions in soil include quartz, calcite and dolomite, which is consistent with the environmental background of the karst geology of the region. Besides, soil contains small amounts of kaolinite and illite. Correspondingly, the main minerals in soil included calcite, quartz and dolomite at points A and B (in the first stage), calcite, quartz, dolomite and illite at points C and D (second stage), and illite, quartz and anorthite at points E and F (third stage; Fig. 5 and Table 1). Meanwhile, the proportions of chlorite, albite and muscovite tended to increase. The enriched Fe or Mg alkaline aqueous environment created beneficial conditions for forming chlorite. At points E and F (long soil-forming time), the compositions and proportions of illite and anorthite increased obviously (Table 1). Chlorite, illite, muscovite, quartz, anorthite and albite increased gradually with the time sequence, while calcite and dolomite tended to decline gradually. Due to long-term weathering and leaching, carbonate rock contents decline or even disappear in aged soil. According to Table 1, the content of quartz tended to increase with time, because quartz remains unchanged during chemical weathering, thus being enriched and reserved. The soil-weathering and soil-forming processes are simultaneous. Meanwhile, chemical weathering of minerals constantly occurs throughout the soil-forming process, and includes original mineral destruction and degradation as well as the generation of new minerals. The macroscopic form, composition and mineralogical properties of soil are consistent.[29] The evolution of mineral associations can indicate soil-forming processes and stages to a certain extent.

5. Conclusions

The evolution of soil aggregation structures is closely related to soil development, the soil-forming process, soil erosion and chemical weathering. As a slope surface evolves, we can see changes in the microstructure of soil, but also migration and changes in biochemical elements and mineral associations. As a whole, the proportions of O, Si and Al were high, while Ca tended to decline along the slope surface and Fe tended to increase. A phenomenon of rich Al and Si contents was extremely obvious. According to the research results, the mineral associations in the soil changed dramatically along the slope surface. The mineral compositions mainly included quartz, calcite and muscovite, which is consistent with the environmental background of karst landforms in the region. The weathering process changed the soil mineral composition. At the bottom of the slope (long soil-forming time), the proportions of illite and anorthite increased significantly. Due to long-term weathering and leaching, carbonate rocks in the soil declined or even disappeared completely.

According to SEM analysis, the evolution of the ultrastructure of soil aggregates is consistent with the evolutionary trends in soil elements and mineralogical properties, with the ultrastructure indicating the soil's developmental stage and condition. The evolution of soil aggregate ultrastructure is consistent with the soil's mineralogical properties, and mineral associations can indicate the soil development stage. The research results in this paper increase our understanding of soil development, soil-forming processes and biogeochemical processes in rocky desertification and karst regions.

Conflicts of interest

There are no conflicts to declare.

Acknowledgements

This work was supported by the Nanyang Normal University Scientific Research Project [grant number ZX2015088]; the Scientific Research and Service Platform Fund of Henan Province [grant number 2016151]; and the National Nature Science Foundation of China [grant number 41601614]. We also thanks for the fund of Scientific and Technological Innovation Team of Water Ecological Security for Water Source Region of Mid-line of South-to-North Diversion Project of Henan Province.

References

1 R. Lal, *Land Degrad. Dev.*, 2001, **12**, 519–539.
2 N. Haregeweyn, J. Poesen, J. Nyssen, J. De Wit, M. Haile, G. Govers and S. Deckers, *Land Degrad. Dev.*, 2006, **17**, 211–230.
3 K. Van Oost, G. Govers and P. Desmet, *Landsc. Ecol.*, 2000, **15**, 577–589.
4 A. Gómez-Plaza, M. Martínez-Mena, J. Albaladejo and V. Castillo, *J. Hydrol.*, 2001, **253**, 211–226.
5 N. Wongfun, J. Götze, G. Furrer, H. Brandl and M. Plötze, *Geoderma*, 2013, **211–212**, 116–127.
6 W. J. Vreeken, *J. Soil Sci.*, 1975, **26**, 378–394.
7 D. H. Yaalon, *Geoderma*, 1975, **14**, 189–205.
8 J. Six, E. T. Elliott and K. Paustian, *Soil Biol. Biochem.*, 2000, **32**, 2099–2103.
9 W. H. Schlesinger, *Nature*, 1990, **348**, 232–234.
10 J. Churchman, *Clay Miner.*, 1980, **15**, 59–76.
11 C. Igwe, M. Zarei and K. Stahr, *Aust. J. Soil Res.*, 2005, **43**, 147–158.
12 C. Mavris, J. Goetze, M. Ploetze and M. Egli, *Sediment. Geol.*, 2012, **280**, 108–118.
13 K. Yoo and S. M. Mudd, *Geoderma*, 2008, **146**, 248–260.
14 J. Tang, X. Tang, Y. Qin, Q. He, Y. Yi and Z. Ji, *Sci. Total Environ.*, 2019, **649**, 1250–1259.
15 A. L. Collins, P. S. Naden, D. A. Sear, J. I. Jones, I. D. L. Foster and K. Morrow, *Hydrol. Process.*, 2011, **25**, 2112–2129.
16 I. Foster, J. Boardman and J. Keay-Bright, *Geomorphology*, 2007, **90**, 126–143.
17 E. Xu, H. Zhang and M. Li, *Sci. Total Environ.*, 2013, **458**, 419–426.
18 J. Lu, F. Zheng, G. Li, F. Bian and J. An, *Soil Tillage Res.*, 2016, **161**, 79–85.
19 C.-A. Haydu-Houdeshell, R. C. Graham, P. F. Hendrix and A. C. Peterson, *Geoderma*, 2018, **310**, 201–208.
20 J. M. Oades and A. G. Waters, *Aust. J. Soil Res.*, 1991, **29**, 815–828.
21 G. S. Zhang and Y. F. Liu, *Sci. Total Environ.*, 2018, **642**, 12–20.
22 D.-M. Zhou, D. Wang, L. Cang, X.-Z. Hao and L. Chu, *J. Soils Sediments*, 2011, **11**, 491–503.
23 N. DeNovio, J. Saiers and J. Ryan, *Vadose Zone J.*, 2004, **3**, 338–351.
24 C. Barton and A. Karathanasis, *Water, Air, Soil Pollut.*, 2003, **143**, 3–21.
25 S. W. Duiker, F. E. Rhoton, J. Torrent, N. E. Smeck and R. Lal, *Soil Sci. Soc. Am. J.*, 2003, **67**, 606–611.
26 Z. Sun, Z. Zhang, K. Zhu, Z. Wang, X. Zhao, Q. Lin and G. Li, *Sci. Total Environ.*, 2019, **708**, 134829.
27 C. J. Bronick and R. Lal, *Geoderma*, 2005, **124**, 3–22.
28 L. E. Parent, C. X. de Almeida, A. Hernandes, J. J. Egozcue, C. Gulser, M. A. Bolinder, T. Katterer, O. Andren, S. E. Parent, F. Anctil, J. F. Centurion and W. Natale, *Geoderma*, 2012, **179**, 123–131.
29 J. Calero, R. Delgado, G. Delgado and J. M. Martín-García, *Eur. J. Soil Sci.*, 2009, **60**, 465–480.
30 S. Anderson, J. Drever, C. Frost and P. Holden, *Geochim. Cosmochim. Acta*, 2000, **64**, 1173–1189.
31 J. Tang, X. Xu, J. Ba and S. Wang, *Chin. Sci. Bull.*, 2010, **55**, 1800–1807.
32 W.-J. Wang, H.-S. He, Y.-G. Zu, Y. Guan, Z.-G. Liu, Z.-H. Zhang, H.-N. Xu and X.-Y. Yu, *Plant Soil*, 2011, **339**, 177–191.
33 J. Elser, M. Bracken, E. Cleland, D. Gruner, W. Harpole, H. Hillebrand, J. Ngai, E. Seabloom, J. Shurin and J. Smith, *Ecol. Lett.*, 2008, **10**, 1135–1142.
34 C. Reynolds and P. Davies, *Biol. Rev. Camb. Philos. Soc.*, 2001, **76**, 27–64.
35 F. Werner, T. Haye, S. Spielvogel and J. Prietzel, *Biogeosci. Discuss.*, 2016, 1–30.